

# Ground Current Control Scheme for Back-to-Back Three-Phase T-Type Rectifier and Inverter Systems

D. O. Boillat\* Non-member, F. Krismer\*\* Non-member  
J. W. Kolar\*\*\* Non-member

(Manuscript received May 15, 2017, revised January 11, 2018)

This paper presents a method to control the ground current in a back-to-back connection of three-phase T-type rectifier and inverter stages, if operated from a three-phase mains with grounded neutral point and a star-connected three-phase load with grounded star-point. The proposed control scheme requires a ground current sensor and a single control loop, achieves a closed-loop control system bandwidth of 1.7 kHz, and does not interact with the existing input phase current control system that is used to achieve sinusoidal mains currents. According to the presented experimental results, an effective reduction of the rms ground current from more than 200 mA (without controller) to less than 3 mA (with the proposed control scheme) is realized.

**Keywords:** Three-Phase, EMI Filter, Ground Current, Common-Mode Equivalent Circuit, System Transfer Function, Control

## 1. Introduction

The Controllable AC Voltage Source (CVS) is a key element of the emerging power-hardware-in-the-loop simulation systems, which are successfully employed in a wide field of applications, for example to analyze power grid dynamics<sup>(1)</sup> or identify implications of grid faults on power electronic systems<sup>(2)(3)</sup>. Due to the versatile use of the CVS, it is required to feature high bandwidth and low output impedance, which can be achieved with the T-type inverter output stage depicted in **Fig. 1**<sup>(4)</sup>, where a fourth bridge-leg provides overmodulation for loads whose star-points are open. A mains-connected PFC T-type rectifier powers the inverter stage of the CVS and it is considered that the star-point of the supplying mains is tied to ground as shown in Fig. 1. The nominal power of the considered CVS is 10 kW and the source is operated from a symmetrical three-phase mains with a nominal phase-to-phase rms voltage of 400 V.

Typical applications of the CVS also include operations with star-connected three-phase loads whose star-points are connected to ground, according to Fig. 1. In this case, minor imprecisions in the generation of the bridge-leg input and output voltages can lead to voltage drops across the input and output filters, which cause a *ground current* due to the present ground connections at the star-points of the mains and the load. This current is of Common Mode (CM) type and can lead to saturation of the CM inductors in the rectifier's EMI filter.

Numerous publications are dedicated to the control of circulating currents that occur in parallel operated inverters, which, besides the CM (zero-sequence) component also con-

tain positive- and negative-sequence components. In this context,<sup>(5)-(7)</sup> present the control of circulating currents in two parallel connected GTO inverters, three-level neutral-point clamped inverters, and back-to-back connections of three-phase PFC rectifier and inverter stages, respectively. Subsequent research focused on generalized mathematical modeling and control of circulating currents<sup>(8)(9)</sup> and the extension of existing models to systems with independent DC-links<sup>(10)</sup>. These investigations, however, commonly focus on inverter systems for motor applications and do not take EMI filters into consideration. With regard to the control of ground currents in inverter systems with dedicated EMI filter, only few documented results exist<sup>(4)(11)(12)</sup>: in<sup>(11)</sup> the ground current is implicitly controlled by controlling the voltage between the negative rail of the DC-link and ground and in<sup>(4)(12)</sup> the ground current is directly measured and controlled. Since the CM inductors of the EMI filter are sensitive to saturation, this work pursues the direct control of the ground current in accordance to<sup>(4)(12)</sup>. However, the concepts presented in<sup>(12)</sup> and<sup>(4)</sup> are based on control structures with three and two cascaded control loops, respectively, and both proposals require two current sensors.

In this paper, in **Section 2**, it is shown that a single loop control structure, which only requires measurements from a single current sensor, facilitates effective control of the ground current, since the losses of the EMI CM inductors provide considerable damping of the filter's resonances. In **Section 3**, a detailed experimental verification of the presented concept is provided. From the obtained measurements, the suggested ground current control scheme is found to not interfere with the input current controllers, i.e., same Total Harmonic Distortion (THD) is measured for the ground current control scheme being inactive or active. The presented control approach achieves an effective reduction of the rms ground current to values less than 3 mA and a closed-

\* ABB Schweiz AG  
Austrasse, 5300 Turgi, Switzerland

\*\* Power Electronic Systems Laboratory, ETH Zurich  
Physikstrasse 3, 8092 Zurich, Switzerland

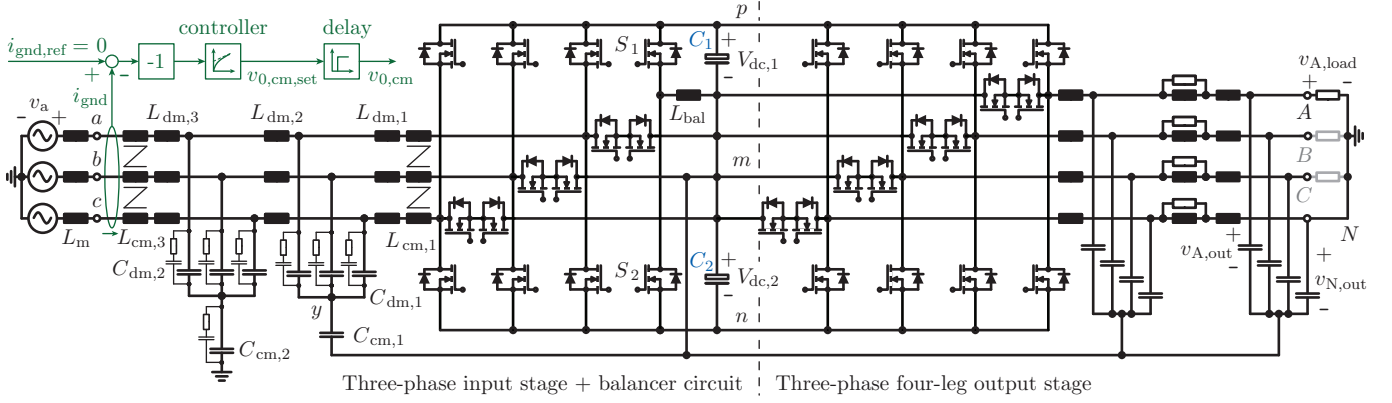


Fig. 1. Controllable AC Voltage Source (CVS) with a three-phase input stage inclusive EMI filter, balancer circuit in the split DC-link ( $S_1$ ,  $S_2$ ,  $L_{bal}$ ), a three-phase four-leg output stage comprising a four-line two-stage LC filter, and a three-phase load with ground-connected star-point. The ground current control loop, with controller and time delay introduced by the power stage, is depicted in the top left-hand corner, where a gain  $-1$  is introduced to correctly account for the defined direction of  $i_{gnd}$ ;  $v_{0,cm, set}$  is added to the setting values of the PWM generators of the three input phases of the rectifier.

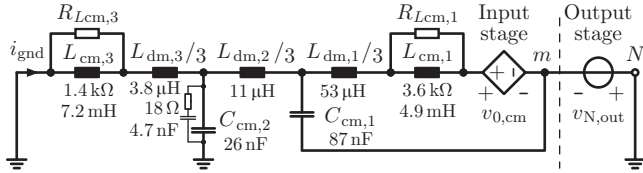


Fig. 2. CM equivalent circuit of the CVS depicted in Fig. 1 for grounded mains star-point, zero mains impedance ( $L_m \rightarrow 0$ ), and grounded load. In addition to Fig. 1,  $R_{Lcm,1}$  and  $R_{Lcm,3}$  are included to model core losses of  $L_{cm,1}$  and  $L_{cm,3}$ ; furthermore,  $C_{dm,1}$  and  $C_{dm,2}$  (and the respective damping branches) are neglected due to comparably low impedances.

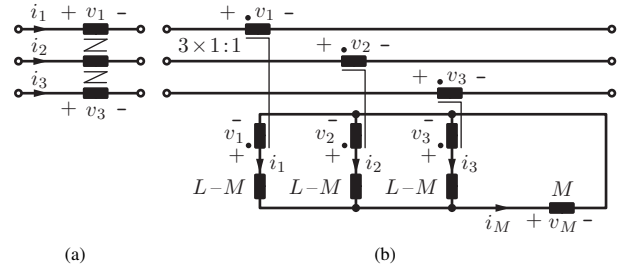


Fig. 3. (a) Three-phase CM inductor; (b) equivalent model of the three-phase CM inductor with its internal model being decoupled by means of three ideal 1:1 transformers.

loop control bandwidth of 1.7 kHz. It can be applied in a straight-forward manner to back-to-back connected three-phase PFC rectifiers and inverters.

## 2. CM Equivalent Circuit and Controller Design

Fig. 2 depicts the system's CM equivalent circuit, which is composed of the CM equivalent circuits of the EMI filter and the rectifier and inverter stages of the CVS. There, the inverter stage is approximated by the voltage source  $v_{N,out}$ , since the output phases are not coupled by means of CM inductors and because the small-signal bandwidth of the output voltage control loop ( $\approx 7$  kHz, cf. <sup>(4)</sup>) is considerably greater than the bandwidth finally achieved for the ground current control loop (1.7 kHz). The capacitors  $C_{dm,1}$  and  $C_{dm,2}$  are neglected, due to  $3C_{dm,1} \gg C_{cm,1}$  and  $3C_{dm,2} \gg C_{cm,2}$ . The two resistors  $R_{Lcm,1}$  and  $R_{Lcm,3}$  consider the implications of the CM inductors' core losses on the frequency response of the EMI filter.

With regard to the CM inductor, no immediately descriptive model is found in literature, which clarifies, how the CM and DM equivalent inductances can be determined for a defined CM inductor with known self inductances and known couplings between its phases. Therefore, this is briefly explained here for the three-phase CM inductor depicted in Fig. 3(a), where

$$v_1 = L_{11}di_1/dt + M_{12}di_2/dt + M_{13}di_3/dt \quad (1)$$

is valid for  $v_1$  and similar expressions apply to  $v_2$  and  $v_3$ . Based on the assumption of a completely symmetric three-phase CM inductor, equal self inductances,  $L = L_{11} = L_{22} = L_{33}$ , and mutual inductances,  $M = M_{mn}$  with  $m, n \in \{1, 2, 3\} \wedge m \neq n$ , can be considered and (1) reduces to

$$v_1 = Ldi_1/dt + M(di_2/dt + di_3/dt), \quad (2)$$

which, after adding  $Mdi_1/dt - Mdi_1/dt = 0$ , can be rearranged to

$$v_1 = (L - M)di_1/dt + Md(i_1 + i_2 + i_3)/dt. \quad (3)$$

Fig. 3(b) depicts the model corresponding to (3) where ideal transformers with turns ratios of 1:1 are used to decouple the physical terminals of the CM inductor from its internal model. With this, the CM and DM equivalent circuits can be directly determined. For CM

$$v_{cm} = v_1 = v_2 = v_3 \wedge i_1 = i_2 = i_3 = i_{cm}/3 \text{ and } k = \frac{M}{L} \rightarrow L_{cm} = (L - M)/3 + M = L(1 + 2k)/3 \quad (4)$$

applies, which is in accordance to the result derived in <sup>(13)</sup>. For DM (positive- and negative-sequence components)  $i_1 + i_2 + i_3 = 0$  needs to be satisfied, from where the inductance per phase,  $L_{dm} = L - M = L(1 - k)$ , is calculated.

According to Fig. 2, both,  $v_{0,cm}$  and  $v_{N,out}$ , can be used to control the ground current. Because the purpose of the

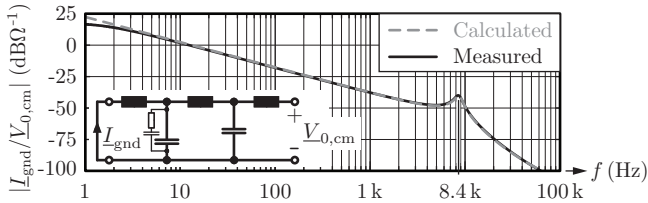


Fig. 4. Measured (black line) and calculated (grey line) CM transfer functions of the *LCLCL* EMI input filter. For the calculated transfer function the measured filter component values as given in Fig. 2 were employed.

CVS is output voltage control, the authors of this work decided to let  $v_{0,cm}$ , i.e., the PFC rectifier stage, control the ground current. This ensures that there are no interactions between the highly dynamic output voltage and the ground current control loops. Since the value of  $v_{N,out}$  is independent of  $i_{gnd}$ ,  $v_{N,out} = 0$  can be considered without restricting the further analysis. Therefore, the transfer function  $\underline{G}_{CVS,cm} = \underline{L}_{gnd}/\underline{V}_{0,cm}$  for  $v_{N,out} = 0$  depicted in Fig. 4 is the one which is relevant for the design of the controller. This transfer function directly results from the CM equivalent circuit of the CVS and has magnitude values in  $\text{dB}\Omega^{-1}$  (reference value is  $1 \Omega^{-1}$ ). In addition, a time delay of the converter of  $16 \mu\text{s}$  (modeled with a first-order Padé approximation) is considered.

In Fig. 4 a difference between measured and calculated transfer functions is observed for very low frequencies,  $f < 10 \text{ Hz}$ , since the inductor's losses are not modeled, there. Within the frequency range relevant for the design of the ground current controller a resonance frequency is observed at  $8.4 \text{ kHz}$ , which is mainly attributed to the weakly damped innermost series resonant circuit formed with  $L_{cm,1}$ ,  $C_{cm,1}$ , and  $R_{Lcm1}$ , cf. Fig. 2.

In principle,  $\underline{G}_{CVS,cm}$  could be solely controlled with a P-controller. However, higher gain (and thus, increased control bandwidth) can be realized if a  $\text{PT}_1$ -element is used to attenuate the filter resonance at  $8.4 \text{ kHz}$ . Furthermore, a PI-controller is employed to achieve increased open-loop gain (and thus, increased disturbance suppression) at low frequencies. Based on these consideration, a  $\text{PI}+\text{PT}_1$ -controller results,

$$\underline{G}_{\text{PI}+\text{PT}_1} = \frac{K_p}{1 + sT} \left( 1 + \frac{1}{sT_i} \right). \quad (5)$$

With  $K_p = 85 \text{ V/A}$ ,  $T = 43 \mu\text{s}$ , and  $T_i = 4.3 \text{ ms}$ , phase and gain margins of  $68^\circ$  and  $15 \text{ dB}$  result, cf. Fig. 5. For the closed loop transfer function a cut-off frequency of  $1.7 \text{ kHz}$  results and the corresponding step response is comparable to that of a second-order low-pass filter with a rise time of  $220 \mu\text{s}$ . Without the  $\text{PT}_1$ -element, i.e., for a conventional PI-controller,  $K_p = 32 \text{ V/A}$  and  $T_i = 1 \text{ ms}$  are determined for similar phase and gain margins of  $68^\circ$  and  $10 \text{ dB}$ . With this, a reduced cut-off frequency of  $580 \text{ Hz}$  results. For this reason, and due to the low additional implementation effort for the  $\text{PT}_1$ -element, the  $\text{PI}+\text{PT}_1$ -controller is preferred in this work.

### 3. Experimental Verification

Given that  $v_{N,out} = 0$  can be considered, cf. Section 2, the

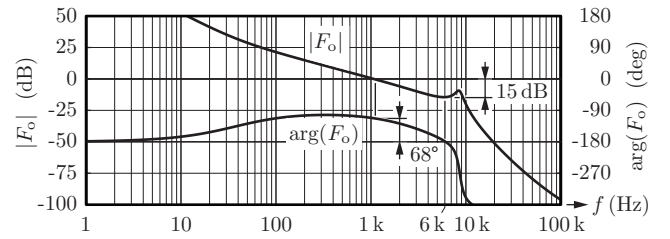


Fig. 5. Gain plot of the open ground control loop transfer function. The selected  $\text{PI}+\text{PT}_1$ -controller enables a gain crossover frequency of  $1.1 \text{ kHz}$  and gain and phase margins of  $15 \text{ dB}$  (at  $f = 6 \text{ kHz}$ ) and  $68^\circ$  (at  $f = 1.1 \text{ kHz}$ ), respectively.

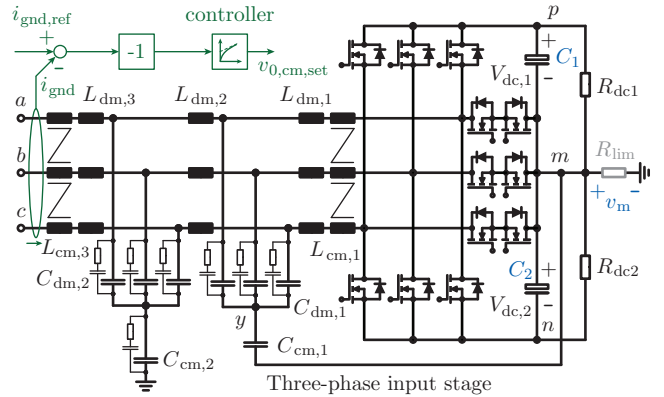


Fig. 6. The three-phase T-type PFC rectifier stage of the CVS used to conduct the experimental verification of the investigated control scheme. The terminal  $m$  is directly connected to ground except for measurements without ground current controller, where a resistor,  $R_{lim} = 1.6 \Omega$ , is used to limit the ground current.

inverter stage of the CVS can be omitted. For this reason, the experimental verification is performed with the three-phase PFC rectifier stage of the CVS depicted in Fig. 6.

All experiments were conducted with a reduced DC-link voltage of  $350 \text{ V}$  and a line-to-line mains voltage with a reduced rms value of  $173 \text{ V}$ . This lowers the risk of a simultaneous saturation of  $L_{cm,1}$  and  $L_{cm,3}$  in case of a deactivated ground current controller, because  $L_{cm,1}$  and  $L_{cm,3}$  saturate at  $100 \text{ Hz}$  at relatively low currents of  $340 \text{ mA}$  and  $65 \text{ mA}$ , respectively. Further details related to the EMI filter components are available in<sup>(4)</sup>. The converter is operated with an output power of  $1.5 \text{ kW}$  and at  $50 \text{ Hz}$  mains frequency. The ground current is measured with LEM's CTSR 0.6-P current sensor, which features the measurement of residual currents with rms values up to  $600 \text{ mA}$ , an accuracy of  $1.5\%$  at an ambient temperature of  $25^\circ\text{C}$ , and a bandwidth of  $9.5 \text{ kHz}$  ( $-1 \text{ dB}$ ). A load resistance of  $2 \times 41 \Omega$  is connected between the  $p$ - and the  $n$ -terminals shown in Fig. 6. The  $m$ -terminal is directly connected to ground, except for measurements without ground current controller, where a resistor,  $R_{lim} = 1.6 \Omega$ , is used to limit the ground current.

Fig. 7 shows different step responses of the closed ground current control loop with reference steps of  $+100 \text{ mA}$  and  $-200 \text{ mA}$ . Except for a slight overshoot of the measured current, which is addressed to the reduced permeability of  $L_{cm,3}$  due to partial saturation, a good matching between simulation and measurement results is obtained.

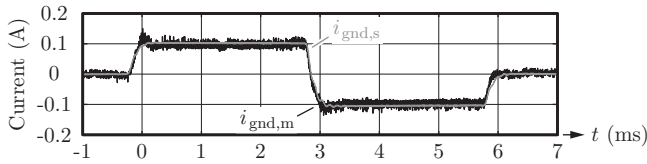


Fig. 7. Measured ( $i_{\text{gnd},m}$ , black curve) and simulated ( $i_{\text{gnd},s}$ , grey curve) ground currents for closed loop operation and different ground current reference steps of +100 mA and -200 mA.

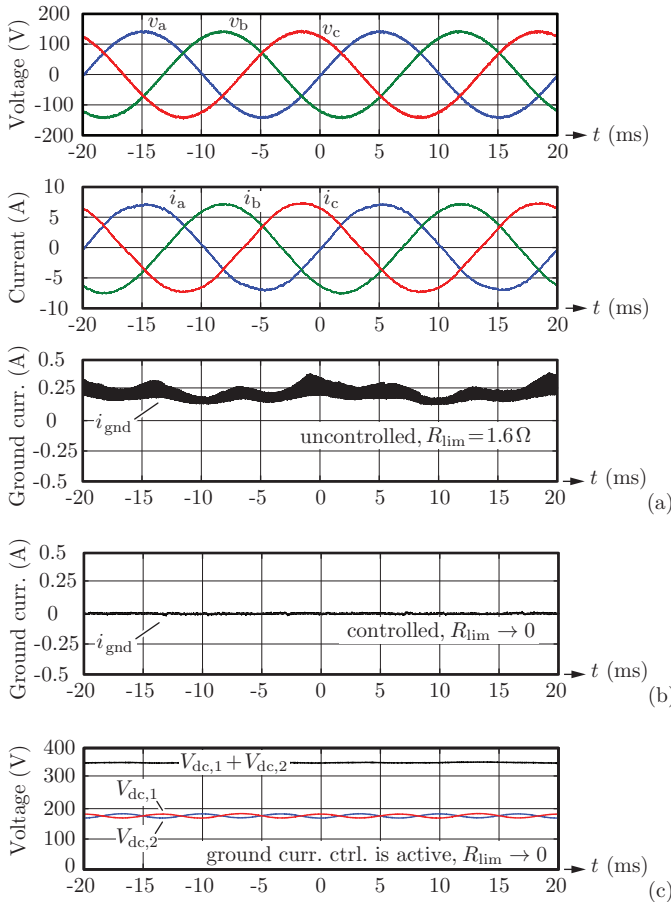


Fig. 8. Experimental results for balanced mains voltages,  $v_a, v_b, v_c$ ; the mains currents  $i_a, i_b, i_c$  and the ground current  $i_{\text{gnd}}$  are measured with the PFC rectifier stage of the CVS depicted in Fig. 1: (a) for deactivated and (b) for activated ground current controller. In (a) a resistance of  $1.6 \Omega$  has been inserted to limit the ground current to reasonable values and in (b) the terminal  $m$  of the PFC rectifier is directly connected to ground. (c) Measured DC-link voltages  $V_{\text{dc},1}$ ,  $V_{\text{dc},2}$ , and  $V_{\text{dc},1} + V_{\text{dc},2}$  (DC-link capacitors:  $C_1 = C_2 = 240 \mu\text{F}$ ).

**Fig. 8** depicts measured phase voltages, phase currents, ground currents for deactivated and activated ground current controller, and DC-link voltages. **Tab. 1** lists the achieved rms values of the ground current, measured with a true rms multimeter, for different values of the output power and for  $R_{\text{lim}} \rightarrow 0$ . The table reveals rms currents of less than 3 mA. Even though  $R_{\text{lim}} = 1.6 \Omega$  has been used in the case of the deactivated ground current controller, a high average current of 220 mA results. This current leads to saturation of  $L_{\text{cm},1}$  and  $L_{\text{cm},3}$  and hence a large current ripple is obtained.

Table 1. Rms values of ground currents at different output power levels, measured with a multimeter (Fluke 175 true rms digital multimeter), for activated ground current controller, and  $R_{\text{lim}} \rightarrow 0$ .

Output power	Ground current
500 W	2.7 mA
750 W	2.5 mA
1 kW	2.5 mA
1.25 kW	2.8 mA
1.5 kW	2.5 mA

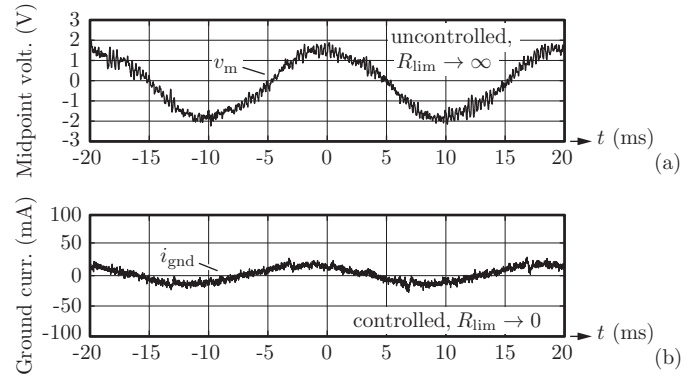


Fig. 9. Experimental results for unbalanced mains voltages,  $V_{\{a,b,c\}} = \{100, 98, 102\} \text{ V}$ : (a) Voltage between the mid-point of the DC-link,  $m$ , and ground for  $R_{\text{lim}} \rightarrow \infty$ ; (b) resulting ground current for activated ground current controller and  $R_{\text{lim}} \rightarrow 0$ .

Same power factors (99.9%), THD values of the phase currents (2.4%), and voltage ripples superimposed on  $V_{\text{dc},1}$  and  $V_{\text{dc},2}$  are measured for activated and deactivated ground current controller. With the employed DC-link capacitances,  $C_1 = C_2 = 240 \mu\text{F}$ , peak to peak voltage ripples of 15 V result for  $V_{\text{dc},1}$  and  $V_{\text{dc},2}$ , cf. Fig. 8(c). For the total DC-link voltage,  $V_{\text{dc},1} + V_{\text{dc},2}$ , a peak to peak voltage ripple of less than 5 V has been measured.

In a final experiment, the ground current control system is tested for an unbalanced three-phase system with rms phase voltages of  $V_{\{a,b,c\}} = \{100, 98, 102\} \text{ V}$  (2% unbalance). **Fig. 9(a)** depicts the CM voltage measured between the mid-point of the DC-link,  $m$ , and ground for  $R_{\text{lim}} \rightarrow \infty$ . Without ground current controller, a sinusoidal CM current with an amplitude of 0.44 A and a frequency of 50 Hz is calculated for this voltage (assuming linear CM filter chokes), which would cause saturation of the CM filter chokes. At 50 Hz the proposed controller features a calculated attenuation of the ground current by 28.5 dB, which leads to a remaining rms ground current of  $0.037 \times (0.44 \text{ A} / \sqrt{2}) = 11.6 \text{ mA}$  for activated ground current controller. The measurement, cf. **Fig. 9(b)**, confirms this result with a measured rms current of 12 mA.

#### 4. Conclusion

The presented work documents the successful control of ground currents for a given three-phase T-type back-to-back PFC rectifier (with EMI filter) and inverter system by means of a single control loop. The proposed control structure is less demanding than the formerly suggested multi-loop structures<sup>(4)(12)</sup> and requires only a single current sensor. In the

course of control design considerations it is found that a controller composed of series-connected conventional PI- and  $PT_1$ -elements is suitable to stabilize the system, since it provides further attenuation to the resonance peaks of the CM filter (in addition to the already present passive attenuation by reason of the losses in the EMI CM inductors). With this, a closed-loop ground current control bandwidth of 1.7 kHz is achieved. Successful operation is experimentally verified in presence of balanced and unbalanced three-phase voltages. The measured rms ground currents are less than 3 mA and 12 mA for balanced and unbalanced supply voltages, respectively. Furthermore, phase current and ground current control systems have been found to operate in parallel and no measurable interactions could be identified.

## References

- (1) J. Wang, L. Yang, Y. Ma, J. Wang, L. Tolbert, F. Wang, and K. Tomsovic, "Static and dynamic power system load emulation in converter-based reconfigurable power grid emulator," *IEEE Trans. Power Electron.*, vol. 31, no. 4, pp. 3239–3251, April 2016.
- (2) J. Eloy-García, J. Vasquez, and J. Guerrero, "Grid simulator for power quality assessment of micro-grids," *IET Power Electron.*, vol. 6, no. 4, pp. 700–709, 2013.
- (3) T. Liu, D. Wang, and K. Zhou, "High-performance grid simulator using parallel structure fractional repetitive control," *IEEE Trans. Power Electron.*, vol. 31, no. 3, pp. 2669–2679, March 2016.
- (4) D. O. Boillat, "Modular high bandwidth switch-mode three-phase AC voltage source," Ph.D. dissertation, Swiss Federal Institute of Technology Zurich (ETH Zurich), 2016.
- (5) F. Tsuchiya, S. Okuma, K. Iwata, "Parallel running of GTO PWM inverters," *Electrical Engineering in Japan*, vol. 104, no. 3, pp. 231–238, April 1984.
- (6) H. Okayama, M. Koyama, T. Ise, "A circulating current control scheme for multiple three-level NPC inverter systems," *Electrical Engineering in Japan*, vol. 136, no. 2, pp. 701–709, May 2000.
- (7) R. Zhang, X. Wu, and T. Wang, "Analysis of common mode EMI for three-phase voltage source converters," *Proc. of the IEEE 34th Power Electronics Specialists Conference (PESC)*, vol. 4, Acapulco, Mexico, 15–19 June 2003, pp. 1510–1515.
- (8) C.-T. Pan and Y.-H. Liao, "Modeling and coordinate control of circulating currents in parallel three-phase boost rectifiers," *IEEE Trans. Industr. Electron.*, vol. 54, no. 2, pp. 825–838, April 2007.
- (9) R. Li and D. Xu, "Parallel operation of full power converters in permanent-magnet direct-drive wind power generation system," *IEEE Trans. Industr. Electron.*, vol. 60, no. 4, pp. 1619–1629, April 2013.
- (10) F. Wang, Y. Wang, Q. Gao, C. Wang, and Y. Liu, "A control strategy for suppressing circulating currents in parallel-connected PMSM drives with individual DC links," *IEEE Trans. Power Electron.*, vol. 31, no. 2, pp. 1680–1691, Feb. 2016.
- (11) F. Chen, R. Burgos, D. Boroyevich, and X. Zhang, "Low-frequency common-mode voltage control for systems Interconnected with power converters," *IEEE Trans. Industr. Electron.*, vol. 64, no. 1, pp. 873–882, Jan. 2017.
- (12) P. Cortés, D. O. Boillat, J. W. Kolar, "Phase-oriented control of a modular 3-phase 3-level 4-leg inverter AC power source supplying floating or grounded loads," *Proc. of the IEEE Energy Conversion Congress and Exposition (ECCE USA)*, Denver, CO, 15–19 Sept. 2013, pp. 1357–1363.
- (13) M. L. Heldwein, "EMC filtering of three-phase PWM converters," Ph.D. dissertation, Swiss Federal Institute of Technology Zurich (ETH Zurich), 2008.

**David O. Boillat** (Non-member) received the M.Sc. degree in electrical engineering and information technology and the Dr. sc. degree from ETH Zurich, Zurich, Switzerland, in 2010 and 2016, respectively. He was an Intern with BKW Group, Bern, Switzerland, in 2009, ABB Corporate Research, Västerås, Sweden, in 2009, and North Carolina State University, Raleigh, NC, USA, in 2010. From 2011 to 2016, he was a Ph.D. Student and a Post-Doctoral Researcher with the Power Electronic Systems Laboratory, ETH Zurich. Since 2017, he has been a Control and Software R&D Engineer with ABB Switzerland Ltd, Turgi, Switzerland. His current research interests include the multi-objective optimal design and realization of high bandwidth switch-mode controllable AC voltage sources employing the newest generation of SiC power semiconductors, high-performance multi-phase power electronic systems, electro-magnetic interference, power semiconductor physics, and modeling and control of power converters and machines.



**Florian Krismer** (Non-member) received the Dipl.-Ing (M.Sc.) degree in electrical engineering from the Vienna University of Technology, Vienna, Austria, in 2004, and the Ph.D. degree in electrical engineering from the Department of Information Technology and Electrical Engineering of ETH Zurich, Zurich, Switzerland, in 2010. He is currently a Research Associate at PES, where he has co-supervised Ph.D. students and has continued with his research in the field of power electronics. He is the author or coauthor of numerous conference and peer-review publications and has received two awards for his publications. His research interests include the analysis, design, and general optimization of power converter systems.



**Johann W. Kolar** (Non-member) is a Fellow of the IEEE and is a Full Professor and the Head of the Power Electronic Systems Laboratory at the Swiss Federal Institute of Technology (ETH) Zurich. He has published over 750 scientific papers in international journals and conference proceedings and has filed more than 140 patents. He received 25 IEEE Transactions and Conference Prize Paper Awards, and the ETH Zurich Golden Owl Award for excellence in teaching. The focus of his current research is on ultra-compact and ultra-efficient SiC and GaN converter systems, wireless power transfer, Solid-State Transformers, Power Supplies on Chip, and ultra-high speed and bearingless motors.

